applied sciences

MDPI

Article

Laser Surface Microtexturing for Enhanced Adhesive Bonding in Steel–Polymer and Steel–Ceramic Joints

Szymon Tofil [1,2,3,*], Leonardo Orazi [4], Vincenzina Siciliani [4], Cyril Mauclair [5], António B. Pereira [6], Sascha Stribick [7], Felix Hartmann [7], Jianhua Yao [3], Qunli Zhang [3], Liang Wang [3] and Shuyang Lin [3]

1 Laser Processing Research Center, Faculty of Mechatronics and Mechanical Engineering, Kielce University of Technology, 7, Av. Tysiąclecia P.P., 25-314 Kielce, Poland
2 Moganshan Institute, Zhejiang University of Technology, Kangqian District, Deqing 313200, China
3 Institute of Laser Advanced Manufacturing, Zhejiang University of Technology, No. 288 Liuhe Road, Liuxia Subdistrict, Xihu District, Hangzhou 310023, China
4 Department of Sciences and Methods for Engineering, Università degli Studi di Modena e Reggio Emilia, 42122 Reggio Emilia, Italy
5 Faculté des Sciences, Université d'Angers, LPHIA, SFR MATRIX, 2 Boulevard de Lavoisier, 49045 Angers CEDEX 01, France
6 TEMA—Centre for Mechanical Technology and Automation, Department of Mechanical Engineering, University of Aveiro, Campus de Santiago, 3810-193 Aveiro, Portugal
7 Fraunhofer Institute for Manufacturing Engineering and Automation IPA, Nobelstraße 12, 70569 Stuttgart, Germany
* Correspondence: tofil@tu.kielce.pl

Featured Application

Laser-based surface microtexturing presented in this study can be applied to the manufacturing of hybrid metal–polymer and metal–ceramic assemblies used in lightweight structural components, industrial housings, and functional elements requiring reliable adhesive bonding. The approach enables improved joint performance without additional mechanical fasteners and is compatible with automated laser processing systems used in industrial production environments.

Abstract

Laser surface microtexturing has emerged as an effective approach for improving the performance of adhesive joints between dissimilar materials. In this study, the influence of laser-generated micrometric surface features on the mechanical behavior of hybrid adhesive joints was investigated for two material systems: structural steel bonded to polyamide (PA66) and structural steel bonded to technical ceramic (Al_2O_3). Single-lap joints were manufactured using a two-component epoxy adhesive with two nominal bond-line thicknesses (0.1 mm and 1.0 mm). Prior to bonding, selected surfaces were modified by ultrashort-pulse laser microtexturing, producing well-defined circular features with characteristic depths on the order of tens of micrometers. The resulting microstructures were characterized using optical and scanning electron microscopy, and their geometric parameters were quantified through profilometric measurements. Mechanical performance was evaluated under shear and bending loading conditions. The results demonstrate a substantial increase in joint strength for laser-microtextured surfaces compared with non-textured references for both material combinations. The effect of surface microtexturing was more pronounced than the influence of adhesive layer thickness within the investigated range. These findings confirm that laser-induced surface microtexturing is a versatile and application-oriented surface preparation method capable of enhancing the reliability of adhesive bonding in hybrid metal–polymer and metal–ceramic assemblies.

Academic Editor: Junseop Lee

Received: 20 February 2026
Revised: 11 March 2026
Accepted: 16 March 2026
Published: 20 March 2026

Keywords: laser surface microtexturing; adhesive bonding; hybrid joints; metal–polymer joints; metal–ceramic joints; surface engineering; mechanical interlocking

1. Introduction

Hybrid material assemblies combining metals with polymers or ceramics have become an integral part of modern industrial manufacturing, driven by the need for lightweight design, functional integration, and improved performance under demanding service conditions. In automotive and transport applications, metal–polymer joints are increasingly used in brackets, housings, and auxiliary structural components to reduce mass and eliminate stress concentrations associated with mechanical fasteners. Similarly, metal–ceramic assemblies are employed in industrial devices where ceramics provide electrical insulation, wear resistance, or thermal stability, while metallic components ensure mechanical load transfer and structural integrity [1,2].

Adhesive bonding is particularly attractive for such hybrid structures because it enables uniform stress distribution, joining of thin-walled components, and compatibility with dissimilar materials that are difficult to weld or mechanically fasten. However, the reliability of adhesive joints strongly depends on surface preparation and process-related parameters, including adhesive selection and bond-line thickness. In dissimilar material systems, limited wetting and insufficient mechanical anchoring at the interface often govern joint failure, highlighting the need for surface engineering approaches that are both effective and compatible with industrial manufacturing constraints [3–13].

Laser-induced surface microtexturing has emerged as a versatile method for tailoring surface topography prior to adhesive bonding. Compared with conventional mechanical or chemical treatments, laser processing enables localized, tool-less, and programmable modification of surface features, supporting automation and high repeatability in manufacturing environments. The use of ultrashort laser pulses further allows precise material removal with limited thermal influence on the surrounding material, which is particularly relevant for hybrid joints involving polymers or ceramics. From an application-oriented perspective, laser surface texturing must nevertheless be evaluated with respect to processing efficiency, energy demand, and potential near-surface effects such as residual stresses, all of which depend on the selected parameter window and material combination [14–25]. In this context, references [14–17] illustrate how laser-generated periodic or hierarchical structures can be used to tailor surface roughness and wettability, providing a physical basis for controlling interfacial phenomena. References [18,19] address the efficiency and process windows of laser-based patterning strategies, which is directly relevant for the practical implementation of surface texturing in industrial environments. Studies [20–25] demonstrate that laser-induced surface structures can significantly enhance adhesion and joint strength, and they highlight the critical role of texture geometry, roughness level, and material pairing in determining the final performance of adhesive joints.

The strengthening of adhesive joints achieved through laser surface texturing is commonly attributed to enhanced mechanical interlocking, resulting from adhesive penetration into microgrooves and cavities, as well as to modified interfacial conditions that promote adhesion. Previous studies on dissimilar material joining—especially metal–polymer systems—have demonstrated that joint performance is sensitive not only to the presence of surface features but also to their geometry, spatial distribution, and the applied loading mode. Consequently, application-relevant investigations should address joint behavior under different mechanical loads while considering manufacturing parameters such as adhesive layer thickness [14–25]. However, the literature does not provide a single universal

set of optimal texture parameters. Reported beneficial ranges of feature depth, spacing, and area coverage vary significantly with the substrate material, adhesive system, and loading mode, which makes it difficult to define global optimum values. In this context, the present study focuses on a well-defined micrometric circular texture and compares textured and non-textured joints under shear and bending, rather than attempting to identify universally optimal microtexture parameters.

Recent reviews on laser surface texturing for adhesive bonding and related interfacial engineering further highlight the diversity of texture geometries, material combinations, and process strategies investigated to date [25]. However, there remains a need for application-oriented studies that directly compare laser-microtextured and non-textured hybrid joints under different loading modes and adhesive layer thicknesses for specific industrially relevant material pairings.

In our earlier studies [26–29], we demonstrated that laser-shaped surface microstructures can significantly increase the strength of adhesive joints and that the magnitude of this improvement depends on microtexture geometry and material pairing. Building on this research line, the present work focuses on two industrially relevant hybrid joints: structural steel (S355JR) bonded to polyamide (PA66) and structural steel bonded to technical ceramic (Al_2O_3). Lap joints were selected to reflect an industry-driven joint configuration commonly used in practical assemblies. The influence of a laser-generated circular microtexture and two adhesive layer thicknesses (0.1 mm and 1 mm) on joint performance is evaluated under shear and bending loading conditions [30–33].

The main contributions of this study are as follows:

(i) A quantitative comparison of laser-microtextured and non-textured interfaces for steel–PA66 and steel–Al_2O_3 lap joints under shear and bending loads;
(ii) An application-oriented assessment of adhesive layer thickness as a technological parameter influencing joint performance;
(iii) Experimental confirmation that the applied laser processing parameters enable effective surface microtexturing without inducing cracking in the investigated materials;
(iv) In contrast to more generic studies on laser-induced roughening, the present work focuses on a well-defined circular microtexture and directly compares its effect on two distinct hybrid joints (steel–PA66 and steel–Al_2O_3) under both shear and bending loads.

From an application perspective, the presented approach is relevant to hybrid assemblies used in lightweight structural components, industrial housings, and functional elements where reliable adhesive bonding of dissimilar materials is required without introducing additional fasteners or complex interlayers. The investigated laser-based surface microtexturing strategy is compatible with automated manufacturing environments and can be adapted to different material combinations and joint geometries. In this context, the following section describes the materials, laser processing parameters, joint configuration, and experimental procedures employed to evaluate the influence of surface microtexturing and adhesive layer thickness on joint performance [34–43].

2. Materials and Methods

2.1. Materials and Specimen Geometry

Structural steel S355JR (according to EN 10025-2, Metinvest Polska, Katowice, Poland) [44,45], polyamide PA66 (PLASTEM, ZDUŃSKA WOLA, Poland) [46], and technical ceramic Al_2O_3 (INN-THERM, Trzcianka, Poland) were used to manufacture hybrid adhesive joints. The specimens were designed as single-lap joints with a nominal overlap length of 12 mm and a specimen thickness of 3 mm, as shown in Figure 1. This joint configuration reflects an industry-driven design commonly used in practical hybrid assemblies.

The chemical composition and mechanical properties of the structural steel are summarized in Tables 1 and 2, respectively.

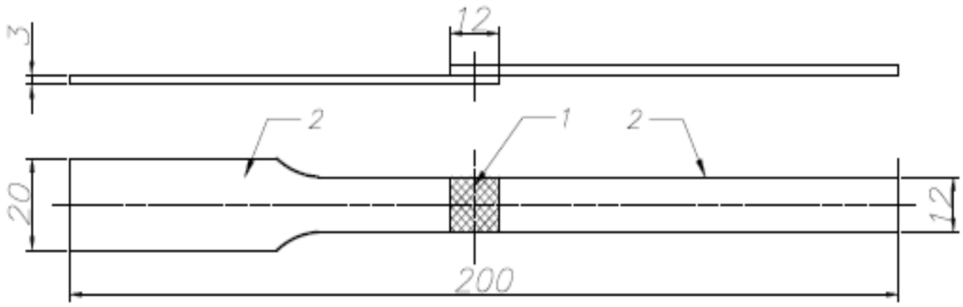

Figure 1. Single-lap joint geometry and dimensions used in this study; 1—laser-textured overlap region; 2—gripping region for mechanical testing (all dimensions in mm).

Table 1. Chemical composition of S355JRsteel [44,45].

C	Mn	Si	P	S	Cu	N	Cr	Ni	Mo	V	Nb	Ti	Al
Max 0.24	Max 1.6	Max 0.55	Max 0.035	Max 0.035	Max 0.55	Max 0.012	-	-	-	-	-	-	-

Table 2. Mechanical properties of S355JR steel [44,45].

Tensile Strength (R_m, MPa)	Yield Strength (R_e, MPa)	Elongation (A80 mm, %)
470–630	≥355	longitudinal samples ≥ 22 transverse samples ≥ 20

2.2. Adhesive System

A two-component epoxy adhesive (MULTIBOND-1101, Multibond Sp. z o.o., Łódź, Poland) [47] was used for all joints. Two nominal adhesive layer thicknesses were investigated: 0.1 mm and 1.0 mm. The adhesive was cured for 24 h under ambient laboratory conditions, in accordance with the manufacturer's recommendations. The main properties of MULTIBOND-1101 are shown in Table 3 [47].

Table 3. Key properties of the MULTIBOND-1101 epoxy adhesive (manufacturer data) [47].

Property	Value	Unit
Viscosity (before it hardens)	10,600 (component A) 6300 (component B)	mPa·s
Specific weight in 25 °C (before it hardens)	1.16 (component A) 0.98 (component B)	g/mL
Shear strength in tensile loading (after it hardens)	26.0 (metals) 7.0 (plastics)	N/mm^2
Peel-off resistance (after it hardens)	5.0	N/mm
Working temperature range	−60 ÷ +100	°C

2.3. Laser Surface Microtexturing

Laser surface microtexturing was performed using an ultrashort-pulse laser system (TruMicro 5325c, TRUMPF, Ditzingen, Germany) operating at a wavelength of 343 nm with a pulse duration of 6.2 ps, an average power of 5 W, and a pulse energy of 12.6 µJ. Beam positioning was achieved using a galvanometer scanning head (intelliSCAN

14, SCANLAB GmbH, Puchheim, Germany). The repetition rate was set to 200 kHz for S355JR steel and 100 kHz for PA66 and Al_2O_3. The laser spot diameter on the sample surface was approximately 40 µm when using a 160 mm focal length F-Theta lens (intelliSCAN 14, SCANLAB GmbH, Puchheim, Germany). The beam scanning speed was set to 150 mm/s for S355JR, 500 mm/s for PA66, and 250 mm/s for Al_2O_3. No line-to-line overlap was applied, and the parameters were selected to ensure stable ablation and consistent formation of the circular microtexture. The laser beam was incident perpendicularly to the sample surface. The laser beam was linearly polarized in all processing conditions. A raster scanning strategy was used to generate the circular microtexture. Laser microtexturing of the steel specimens was performed in an argon shielding atmosphere with a continuous gas flow to stabilize the ablation process and minimize oxidation. In contrast, PA66 and Al_2O_3 were processed in ambient air, which effectively facilitated the removal of ablated material from the interaction zone.

For each investigated material, the number of raster scans was selected experimentally to achieve stable ablation and reproducible microtexture formation. Several geometric variants were evaluated during the broader research project, while the present study focuses on the representative microtexture parameters listed in Table 4. The pulse duration, wavelength, average power, pulse energy and spot size were identical for all materials, while the repetition rate and scanning speed were adjusted individually for steel, PA66 and Al_2O_3 as specified above. A schematic of the laser processing setup is shown in Figure 2. In all joint configurations, both adherends were laser-textured within the overlap region. Only the reference samples were bonded without any surface texturing. Reference samples underwent the same cleaning procedure as the textured specimens. Prior to bonding, the surfaces were degreased with ethanol, dried with warm air, and handled under identical ambient laboratory conditions. No laser processing was applied to these samples.

Table 4. Measured geometric parameters of a representative laser-generated microtexture element.

The Measured Value	Unit of Measurement	Measurement Value
Height	µm	92.448
Width	µm	919.305
Volume	μm^3	3.42×10^8

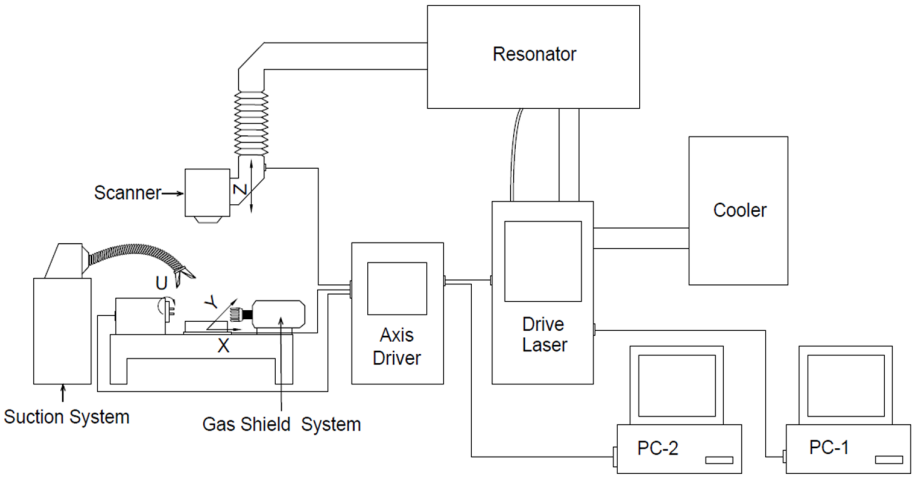

Figure 2. Schematic of the laboratory setup used for laser surface microtexturing (TruMicro 5325c with galvanometer scanning head).

Prior to processing, specimen surfaces were degreased with ethanol and dried with warm air. All samples were stored under ambient laboratory conditions (22–24 °C,

40–50% RH) prior to laser texturing. After laser processing, the samples were cleaned in an ultrasonic bath using ethanol followed by deionized water.

Two types of microstructures were generated within the overlap area: parallel microgrooves oriented perpendicular to the loading direction and a circular microtexture. The parallel grooves were produced with an average spacing of approximately 80 μm and an average depth of about 30 μm. The circular microtexture covered approximately 50% of the bonding surface, with a characteristic diameter of about 1 mm and an average depth of approximately 90 μm. The density and distribution of the microstructures were selected based on empirical optimization performed in previous studies by the authors [26–29]. After laser machining and cleaning, the samples were stored under ambient laboratory conditions (22–24 °C, 40–50% RH) for less than 24 h before adhesive bonding, consistent with observations on the stabilization of laser-structured surfaces reported in [48].

The circular microtexture was selected as a representative geometry providing a balance between pronounced mechanical interlocking and feasible processing time. The feature diameter (~1 mm), depth (~90 μm), and areal coverage (~50% of the overlap region) were chosen based on preliminary trials and previous studies by the authors [26–29], which indicated that such dimensions promote adhesive penetration and load transfer without inducing cracking or excessive stress concentration in the substrates.

2.4. Joint Fabrication and Bond-Line Thickness Control

After laser processing and cleaning, lap joints were fabricated using a dedicated fixture enabling simultaneous assembly of five specimens. Both adherends were positioned in the fixture after laser texturing. Bond-line thickness was controlled using spacer inserts providing nominal thicknesses of 0.1 mm and 1.0 mm. After adhesive application and assembly, the joints were maintained in the fixture under pressure until full curing. The fixture used for joint assembly and bond-line thickness control is shown in Figure 3. Figure 3 presents photographs of the specimens during the subsequent stages of the bonding process using the dedicated fixture that stabilizes the relative position of the adherends. In Figure 3A, the first adherend is positioned and fixed in the holder; in Figure 3B, the spacer insert is placed between the adherends and the adhesive is applied; in Figure 3C, the second adherend is positioned against the spacer and clamped in the overlap region. The fixture allows simultaneous bonding of five specimens, while the spacer insert ensures the nominal adhesive layer thickness (0.1 or 1.0 mm). After adhesive application, the specimens remained immobilized in the fixture until full curing (approximately 24 h, according to the manufacturer's recommendations). The selected nominal bond-line thicknesses of 0.1 mm and 1.0 mm reflect two application-relevant extremes: a thin adhesive layer representative of high-precision assemblies and a thicker layer representative of industrial joints with higher tolerance requirements. The actual bond-line thickness was verified on representative cross-sections prepared from additional specimens, confirming deviations below ± 0.02 mm for the 0.1 mm configuration and below ± 0.05 mm for the 1.0 mm configuration. These tolerances are consistent with the mechanical fixture design and ensure that the observed differences in joint performance are not attributable to uncontrolled variations in adhesive thickness.

In the schematic shown in Figure 3D, elements (1) and (3) represent the laser-textured adherends, (2) denotes the adhesive layer, and (4) indicates the textured overlap region on both bonded surfaces. The arrows illustrate the applied clamping pressure. The fixture was designed to accommodate different adhesive layer thicknesses as well as variations in the size and geometry of the joined components.

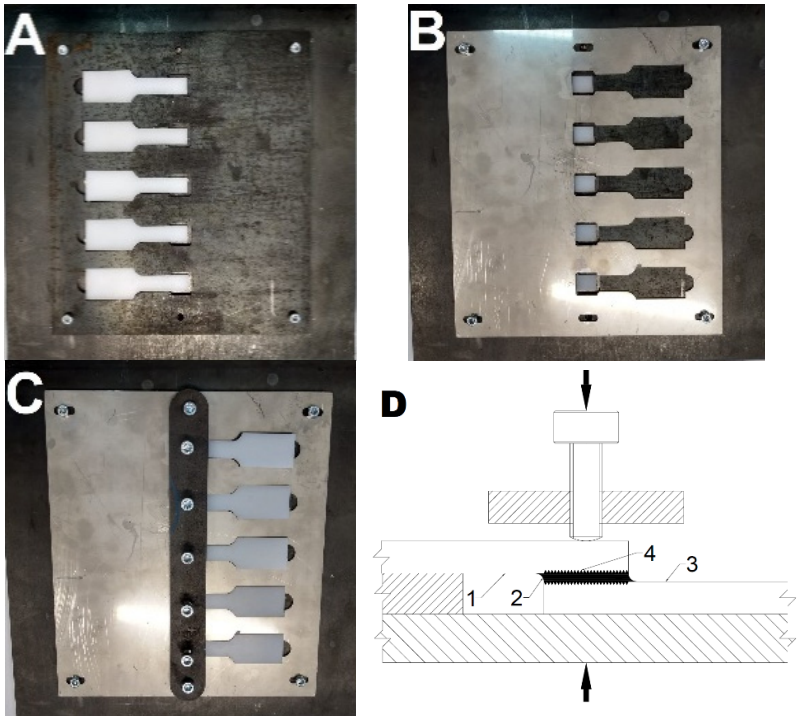

Figure 3. Dedicated fixture for lap-joint assembly and bond-line thickness control: (**A**) positioning of the first adherend; (**B**) adhesive application with spacer insert; (**C**) positioning of the second adherend and clamping during curing; and (**D**) the schematic of the joint showing the textured area and applied pressure.

2.5. Mechanical Testing

Mechanical tests were carried out using a universal testing machine (Instron 4502, Norwood, MA, USA). The specimens were prepared and tested in accordance with the general requirements of the PN-EN ISO 6892-1 standard [49,50], adapted for adhesive lap joints. Joint performance was evaluated under shear and bending loading conditions. For each variant, five specimens were tested. The maximum force at failure was determined for each specimen, and the values reported in the results correspond to the arithmetic mean of these five measurements.

All mechanical tests were performed under displacement control. For the shear tests, a constant crosshead speed of 1 mm/min was applied. The bending tests were carried out in a three-point configuration, with the load applied at a single central point and the supports positioned symmetrically at the specimen ends. In the bending setup, the steel adherend was located on the tensile side of the joint, while the PA66 or Al_2O_3 adherend was subjected to compression. This configuration was selected to reflect typical loading conditions in hybrid structural components.

3. Results

Laser surface microtexturing was applied to the overlap region of the specimens prior to bonding. Representative views of the resulting surface features on steel and ceramic are shown in Figure 4 (HIROX KH-8700 digital microscope, Hirox Co., Ltd., Tokyo, Japan) and Figure 5 (JEOL 7100f scanning microscope, JEOL Ltd., Tokyo, Japan), respectively. The images are representative and intended to illustrate the morphology of the circular microtexture.

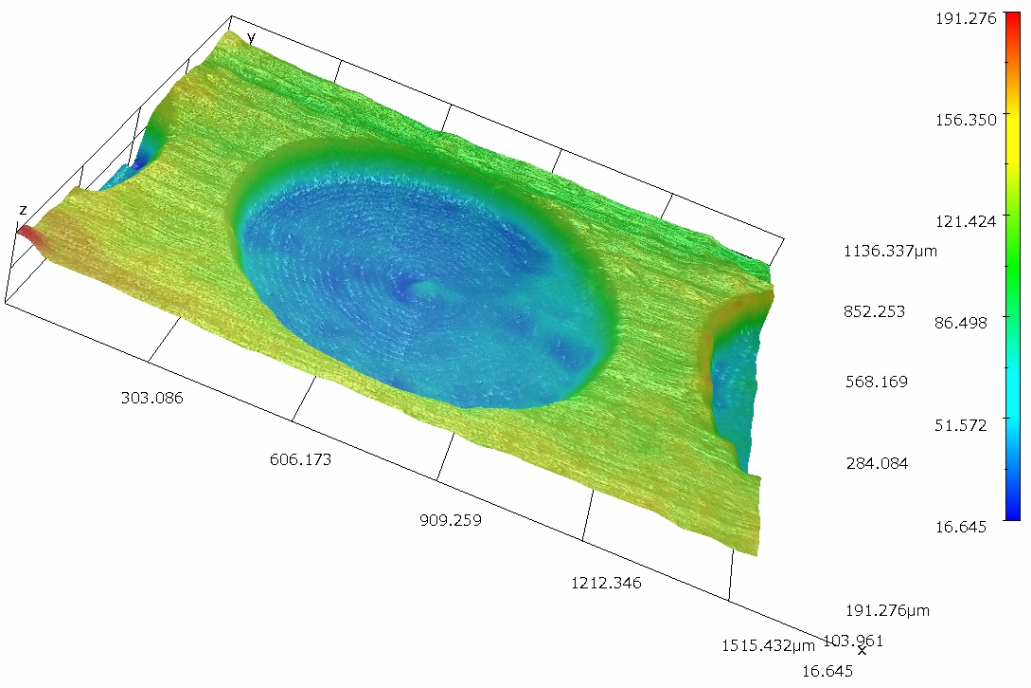

(**a**)

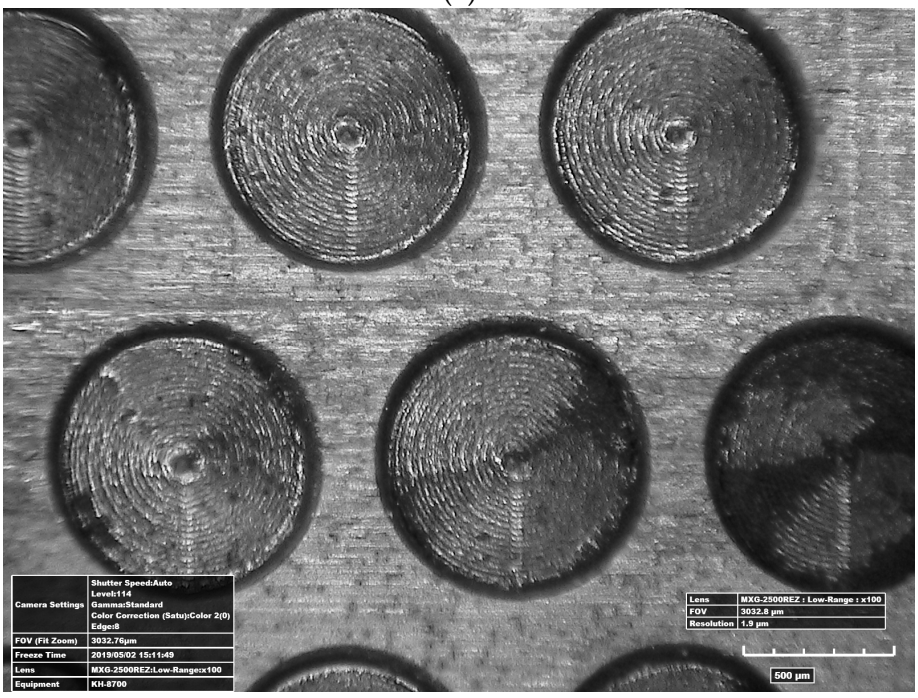

(**b**)

Figure 4. (**a**) Representative optical microscope image of a single laser-generated circular microtexture element on the steel surface, shown in pseudocolor to highlight its topographical relief (HIROX KH-8700). (**b**) Optical microscope view of a textured region within the overlap area, illustrating the spatial distribution and uniformity of the circular microtexture pattern (HIROX KH-8700).

Due to the different material response during ablation, the ceramic surface exhibits a distinct morphology compared with steel. The SEM image is representative and intended to illustrate the morphology of the microtexture on Al_2O_3. The quantitative geometric parameters used in the analysis were obtained from profilometric measurements (Table 4), as the ablation footprint naturally differs between materials due to their distinct optical and thermal properties.

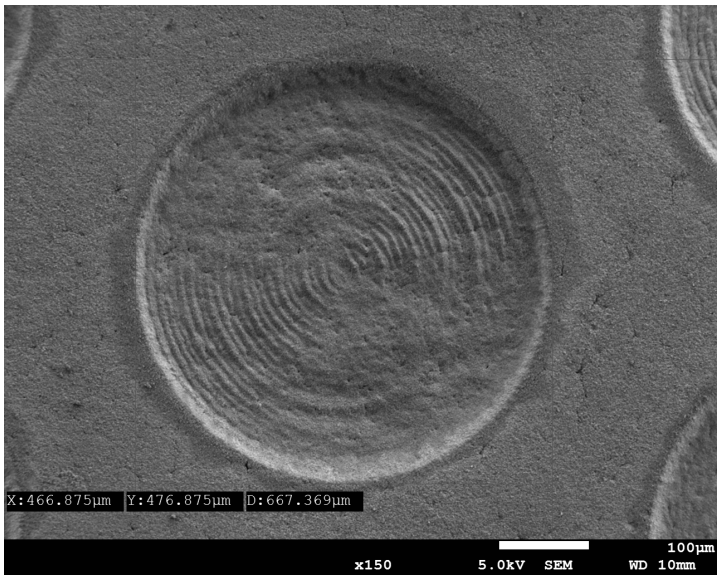

(**a**)

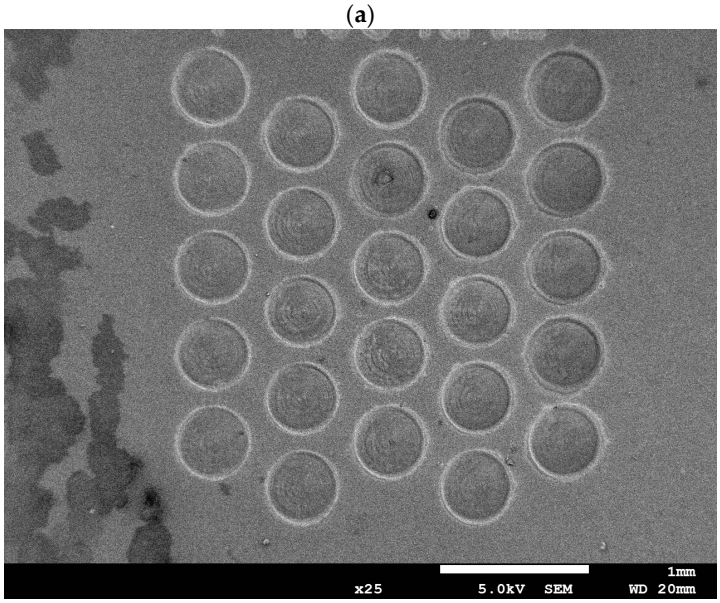

(**b**)

Figure 5. (**a**) SEM image of a single laser-generated circular microtexture element on the Al_2O_3 ceramic surface, showing the characteristic topography of the ablated region (JEOL JSM-7100F). (**b**) SEM view of a representative textured area within the overlap region, illustrating the spatial distribution and uniformity of the circular microtexture pattern (JEOL JSM-7100F).

3.1. Microtexture Geometry and Surface Characterization

To quantify the geometric characteristics of the laser-generated microtextures, selected surface features were analyzed using optical and scanning electron microscopy. The measurements focused on characteristic dimensions of individual texture elements, providing a quantitative basis for correlating surface morphology with joint performance.

The values reported in Table 4 correspond to representative measurements of individual texture elements. Multiple features were inspected to confirm repeatability; however, a full statistical analysis of measurement uncertainty was not included in the present study.

The images presented in Figures 4–7 are representative and intended to illustrate the morphology of the microtexture. All quantitative geometric parameters used in the analysis were obtained from profilometric measurements (Table 4). Profilometric data were extracted using the built-in measurement software (V_8.01) of the HIROX KH-8700 system.

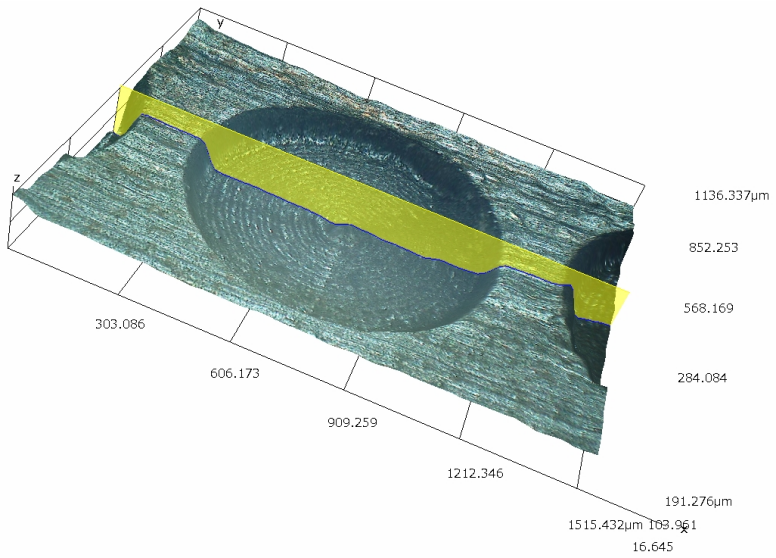

(**a**)

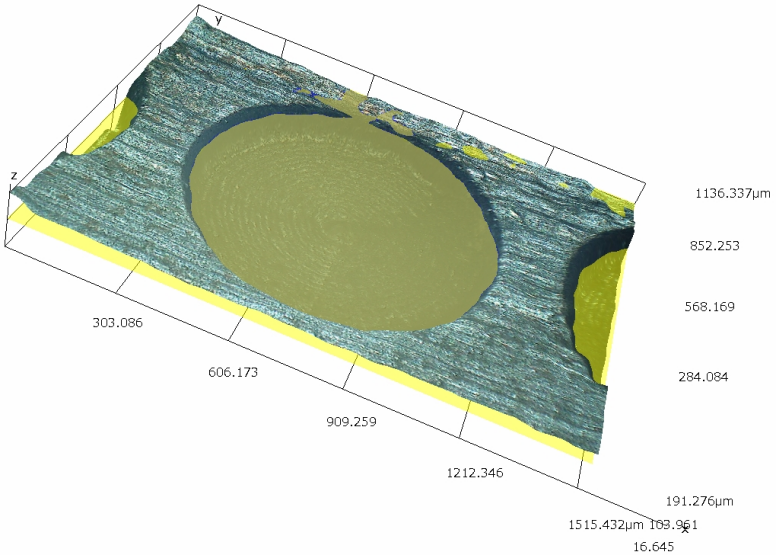

(**b**)

Figure 6. (**a**) Transverse profile of a single laser-generated circular microtexture element on the steel surface, extracted using the built-in measurement software of the HIROX KH-8700 digital microscope. (**b**) Three-dimensional reconstruction and volume estimation of the same microtexture element, obtained from the profilometric dataset acquired with the HIROX KH-8700 system.

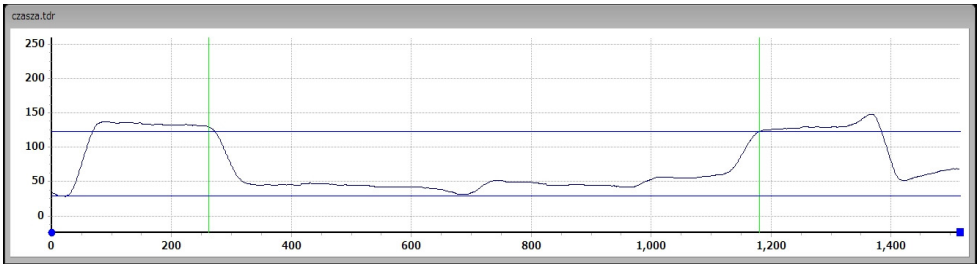

Figure 7. Cross-sectional profile of a representative laser-generated circular microtexture element, obtained from the profilometric dataset acquired with the HIROX KH-8700 digital microscope. The profile illustrates the characteristic depth and shape used for geometric evaluation.

The measurements indicate that the laser-generated microtexture exhibits well-defined and repeatable geometric features. The characteristic height and width of individual

texture elements confirm the formation of pronounced surface relief, while the measured volume reflects the material removal achieved during laser processing. These geometric characteristics are expected to promote mechanical interlocking between the adhesive and the textured surface, contributing to enhanced joint performance. At higher magnification, local nanometric ripples (LIPSS) may be present on the ablated surfaces; however, these features were not systematically analyzed in this study, and the present work focuses on the dominant micrometric topography. Although Ra was not measured directly, the peak-to-valley height estimated from the false-color topography in Figure 4 is approximately 20–40 µm, which is consistent with the simulated values reported in [51]. In addition to topographical modification, laser processing also influenced the wetting behavior of the investigated materials. For example, the contact angle on S355JR increased from 92° (reference) to values between 108° and 136° depending on the microtexture geometry, while Al_2O_3 showed a decrease from 54° (reference) to 50–75° for most patterns. These results confirm that laser texturing modifies both surface morphology and surface energy, which may additionally contribute to improved adhesion.

3.2. Mechanical Performance of Adhesive Joints

The mechanical performance of the adhesive joints was evaluated under shear and bending loading conditions. The influence of laser surface microtexturing and adhesive layer thickness on joint strength was assessed for steel–PA66 and steel–Al_2O_3 material combinations.

As shown in Figures 8 and 9, laser surface microtexturing leads to a pronounced increase in the maximum shear force for both investigated material combinations. The effect is observed for both adhesive layer thicknesses, indicating that surface condition plays a dominant role in joint performance under shear loading. The corresponding average values of the maximum shear force are summarized in Table 5.

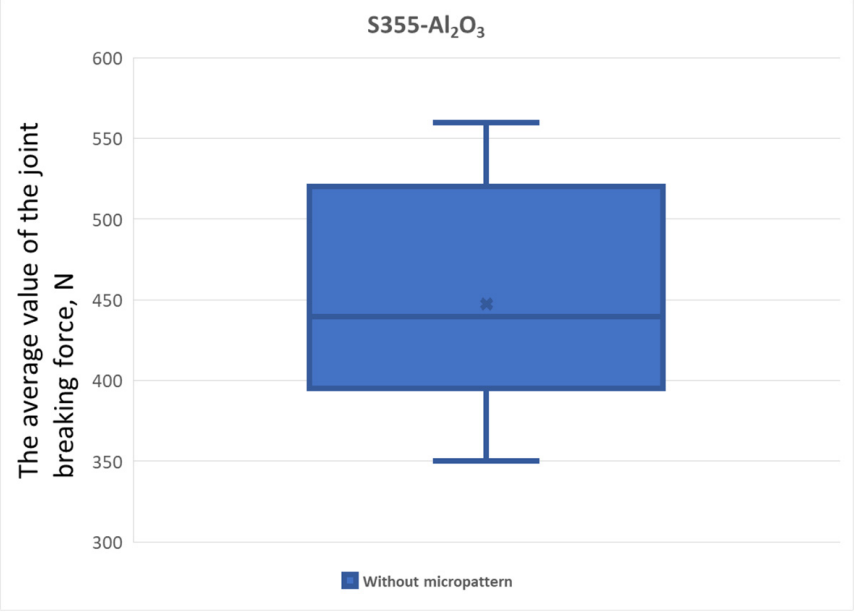

(a)

Figure 8. *Cont.*

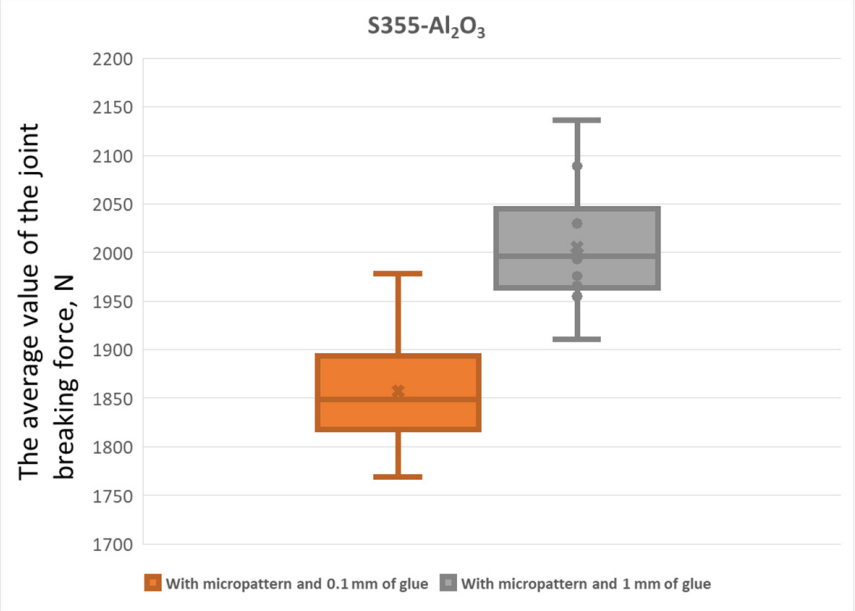

(**b**)

Figure 8. (**a**) Maximum shear force of the S355–Al_2O_3 adhesive joints without laser-generated microtexture, shown for different surface conditions and adhesive layer thicknesses. (**b**) Maximum shear force of the S355–Al_2O_3 adhesive joints with laser-generated circular microtexture, presented separately for adhesive layer thicknesses of 0.1 mm and 1 mm to illustrate the influence of bondline thickness on joint performance.

Table 5. Average values of the maximum shear force required to break the adhesive joints.

Joint Type	The Shear Force [N]		
	Without Micropattern	With Micropattern and 0.1 mm of Glue	With Micropattern and 1 mm of Glue
S355-Al_2O_3	447	1857	2006
S355-PA66	504	1764	1857

The results indicate a substantial increase in shear strength for joints manufactured on laser-microtextured surfaces compared with non-textured references. For both material combinations, higher shear forces were recorded for textured specimens, with a moderate influence of adhesive layer thickness observed within the investigated range.

Figures 10 and 11 present the maximum bending force required to cause joint failure. Similarly to the shear tests, laser-microtextured surfaces exhibit significantly higher bending strength compared with non-textured references for both material systems.

Table 6. Average values of the maximum bending force required to break the adhesive joints.

Joint Type	The Bending Force [N]		
	Without Micropattern	With Micropattern and 0.1 mm of Glue	With Micropattern and 1 mm of Glue
S355-Al_2O_3	15.55	91.33	97.66
S355-PA66	23.2	52.7	54.7

Similar trends were observed under bending loading conditions. Laser surface microtexturing resulted in a pronounced increase in the bending force required to cause joint failure for both material combinations. The effect of adhesive layer thickness was less pronounced than the influence of surface texturing.

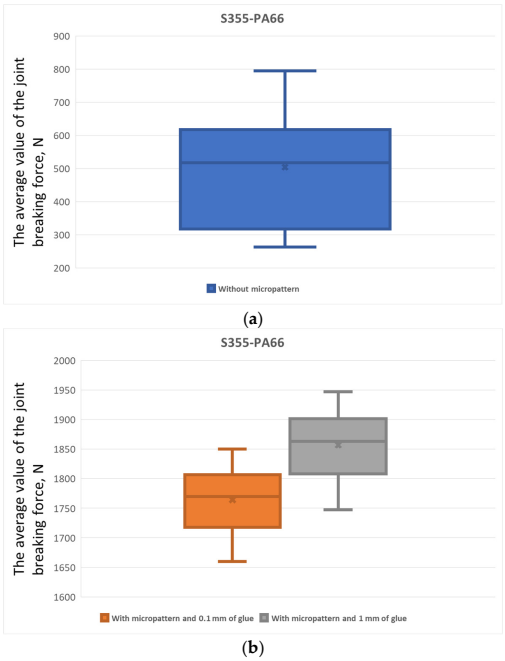

Figure 9. (**a**) Maximum shear force of the S355–PA66 adhesive joints without laser-generated microtexture, shown for different surface conditions and adhesive layer thicknesses. (**b**) Maximum shear force of the S355–PA66 adhesive joints with laser-generated circular microtexture, presented separately for adhesive layer thicknesses of 0.1 mm and 1 mm to illustrate the influence of bondline thickness on joint performance.

Average values of the maximum bending force obtained for the tested joints are listed in Table 6.

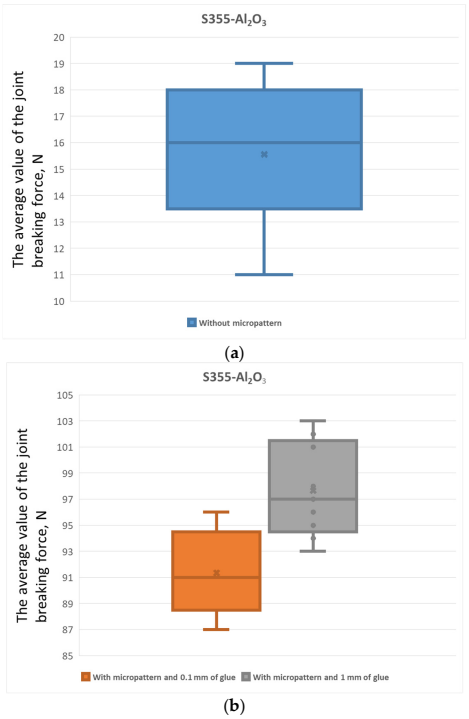

Figure 10. (**a**) Maximum bending force of the S355–Al_2O_3 adhesive joints without laser-generated microtexture, shown for different surface conditions and adhesive layer thicknesses. (**b**) Maximum bending force of the S355–Al_2O_3 adhesive joints with laser-generated microtexture, presented separately for adhesive layer thicknesses of 0.1 mm and 1 mm to illustrate the influence of bondline thickness on joint performance.

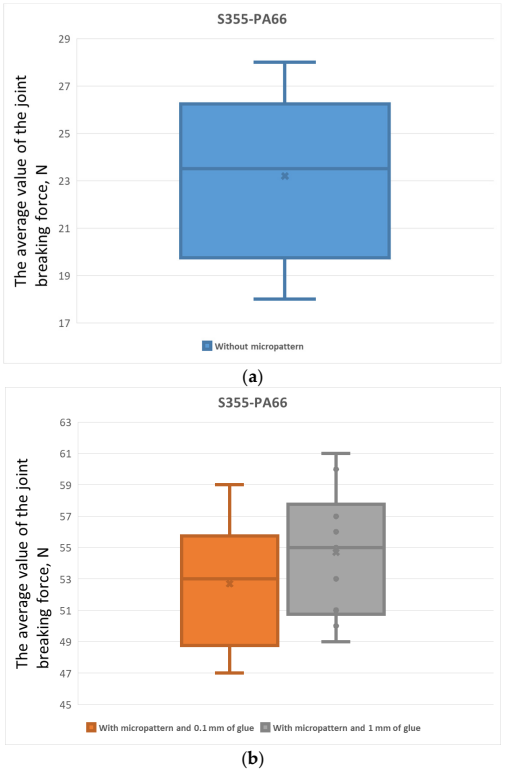

Figure 11. (**a**) Maximum bending force of the S355–PA66 adhesive joints without laser-generated microtexture, shown for different surface conditions and adhesive layer thicknesses. (**b**) Maximum bending force of the S355–PA66 adhesive joints with laser-generated microtexture, presented separately for adhesive layer thicknesses of 0.1 mm and 1 mm to illustrate the influence of bondline thickness on joint performance.

4. Discussion

4.1. Effect of Laser Surface Microtexturing on Joint Performance

The results clearly demonstrate that laser surface microtexturing significantly enhances the mechanical performance of adhesive joints for both investigated material combinations [52–55]. The presence of well-defined micrometric microstructures on the bonding surfaces promotes mechanical interlocking between the adhesive and the substrate, which is reflected in increased shear and bending forces at failure. While additional effects related to laser-induced changes in surface chemistry cannot be excluded, the present study was designed and interpreted primarily in terms of micrometric topography. In particular, ultrashort-pulse laser processing may locally modify oxide layer thickness, surface energy, and wetting behavior, as also suggested by the contact angle changes reported in Section 3.1. However, a detailed chemical or spectroscopic analysis was beyond the scope of this work, and the present interpretation focuses on the dominant contribution of micrometric surface relief and mechanical interlocking. This trend is particularly evident when comparing the textured joints with the reference samples, where the absence of microstructures results in substantially lower shear and bending strength. This effect is consistent with the geometric characteristics of the microtextures described in Section 3.1, where pronounced surface relief and repeatable feature dimensions were observed.

In the present study, the focus was placed on a controlled circular microtexture rather than on uniformly laser-roughened surfaces. Although uniform laser roughening can also increase surface area and roughness, our previous exploratory trials indicated that discrete, well-defined microfeatures provide a more direct link between texture geometry and joint performance, which motivated the choice of the patterned microtexture investigated here.

4.2. Influence of Adhesive Layer Thickness

Within the investigated range, the influence of adhesive layer thickness on joint strength was less pronounced than the effect of surface microtexturing [23–28,35–37]. Although differences between the 0.1 mm and 1.0 mm adhesive layers were observed, the overall trends indicate that surface condition plays a dominant role in determining joint performance. The influence of adhesive layer thickness was comparatively minor, indicating that microtexture-induced mechanical interlocking plays a more decisive role than the nominal bond-line thickness. From a practical perspective, this suggests that laser surface preparation may offer greater performance gains than increasing adhesive consumption.

4.3. Comparison with Previous Studies

The observed improvement in joint performance is in good agreement with previous studies reporting enhanced adhesion due to laser-induced surface structuring [26,27,30,37,38]. Similar trends have been reported for metal–polymer systems, where micro- and nano-scale surface features were shown to improve mechanical interlocking and joint strength. Recent investigations also emphasize that the effectiveness of laser surface treatment depends on both texture geometry and loading mode, which is consistent with the present findings for shear and bending conditions. The results obtained in this study further extend these observations to metal–ceramic joints, highlighting the versatility of laser-based surface engineering for hybrid assemblies.

4.4. Application-Oriented Implications and Limitations

From an application-oriented perspective, the presented results indicate that laser surface microtexturing can be effectively used to improve the performance of hybrid adhesive joints without introducing additional mechanical fasteners or complex interlayers. The applied processing strategy is compatible with automated laser systems and can be adapted to different material combinations and joint geometries. At the same time, the study is limited to static loading conditions and selected texture geometries. Further investigations addressing fatigue behavior, environmental durability, and alternative microtexture designs are required to fully assess the long-term performance of such joints in industrial applications. Future work may also explore process acceleration through multi-spot beam shaping, as discussed in recent reviews on laser spatial beam shaping [51].

5. Conclusions

This study demonstrates that laser-induced surface microtexturing is an effective method for enhancing the mechanical performance of adhesive joints between dissimilar materials. Based on the experimental results obtained for steel–PA66 and steel–Al_2O_3 lap joints, the following conclusions can be drawn:

1. Laser surface microtexturing leads to a substantial increase in both shear and bending strength compared with non-textured reference surfaces for both investigated material combinations.
2. The improvement in joint performance is consistent with the formation of well-defined and repeatable microstructures, which promote mechanical interlocking between the adhesive and the textured substrate.
3. Within the investigated range, the influence of adhesive layer thickness is less pronounced than the effect of surface microtexturing, indicating that microtexture-induced mechanical interlocking plays a more decisive role than the nominal bond-line thickness.

4. The applied ultrashort-pulse laser processing parameters enabled the generation of stable microtextures without inducing cracking or thermal damage, confirming the suitability of this approach for hybrid metal–polymer and metal–ceramic assemblies.

Overall, the results highlight the potential of laser surface microtexturing as a robust and application-oriented surface preparation method for improving the reliability of adhesive bonding in lightweight structural components and functional hybrid assemblies.

Author Contributions: Conceptualization, S.T.; methodology, S.T.; investigation, S.T.; formal analysis, S.T.; data curation, S.T.; writing—original draft preparation, S.T.; writing—review and editing, A.B.P., S.S., F.H., L.O., V.S., J.Y., Q.Z., L.W., S.L. and C.M.; supervision, A.B.P., L.O., J.Y., Q.Z. and L.W.; resources, S.S., F.H., J.Y., Q.Z. and L.W.; validation, S.T., A.B.P. and L.O.; visualization, S.T.; project administration, S.T. All authors have read and agreed to the published version of the manuscript.

Funding: This research was funded by the Polish National Centre for Research and Development (NCBiR, Poland), grant number LIDER/30/0170/L-8/16/NCBR/2017.

Institutional Review Board Statement: Not applicable.

Informed Consent Statement: Not applicable.

Data Availability Statement: The data presented in this study are available from the corresponding author upon reasonable request.

Conflicts of Interest: The authors declare no conflicts of interest.

References

1. Cole, G.S.; Sherman, A.M. Light-weight materials for automotive applications. *Mater. Charact.* **1995**, *35*, 3–9. [CrossRef]
2. Adams, R.D.; Wake, W.C. *Structural Adhesive Joints in Engineering*; Elsevier Applied Science Publishers: London, UK; New York, NY, USA, 1984; pp. 19–23.
3. Rudawska, A. *Wybrane Zagadnienia Konstytuowania Połączeń Adhezyjnych Jednorodnych i Hybrydowych*; Politechnika Lubelska: Lublin, Poland, 2013; pp. 115–130.
4. Rudawska, A.; Chruściel, M. Wpływ sposobu przygotowania powierzchni na wytrzymałość połączeń klejowych lotniczego stopu aluminium. *Technol. Autom. Montażu* **2011**, *2*, 42–46.
5. Broughton, W.; Crocker, L.; Urquhart, J. *Strength of Adhesive Joints: A Parametric Study*; NPL: Teddington, UK, 2001.
6. Rudawska, A. Wytrzymałość połączeń klejowych blach tytanowych po różnych sposobach przygotowania powierzchni. *Inżyniera Mater.* **2009**, *5*, 341–345.
7. Godzimirski, J.; Kozakiewicz, J.; Łunarski, J.; Zielecki, W. *Konstrukcyjne Połączenia Klejowe Elementów Metalowych w Budowie Maszyn*; Oficyna Wydawnicza Politechniki Rzeszowskiej: Rzeszów, Poland, 1997.
8. Kah, P.; Suoranta, R.; Martikainen, J.; Magnus, C. Techniques for joining dissimilar materials: Metals and polymers. *Adv. Mater. Sci.* **2014**, *3*, 152–164.
9. Rozovskis, G.; Vinkevičius, J.; Jačiauskiene, J. Plasma surface modification of polyimide for improving adhesion to electroless copper coatings. *J. Adhes. Sci. Technol.* **1996**, *10*, 399–406. [CrossRef]
10. Kennedy, A.C.; Kohler, R.; Poole, P. A sodium hydroxide anodize surface pretreatment for the adhesive bonding of titanium alloys. *Int. J. Adhes. Adhes.* **1983**, *3*, 133–139. [CrossRef]
11. Rechner, R.; Jansen, I.; Beyer, E. Influence on the strength and aging resistance of aluminium joints by laser pre-treatment and surface modification. *Int. J. Adhes. Adhes.* **2010**, *30*, 595–601. [CrossRef]
12. Ingram, C.; Ramani, K. The effect of sodium hydroxide anodization on the durability of poly(etherketonetherketoneketone) adhesive bonding of titanium. *Int. J. Adhes. Adhes.* **1997**, *17*, 39–45. [CrossRef]
13. Johnsen, B.B.; Lapique, F.; Bjorgum, A. The durability of bonded aluminium joints: A comparison of AC and DC anodising pretreatments. *Int. J. Adhes. Adhes.* **2004**, *24*, 153–161. [CrossRef]
14. Shen, M.X.; Zhang, Z.X.; Yang, J.T.; Xiong, G. Wetting behavior and tribological properties of polymer brushes on lasertextured surface. *Polymers* **2019**, *11*, 981. [CrossRef]
15. Prakash, C.G.J.; Prasanth, R. Approaches to design a surface with tunable wettability: A review on surface properties. *J. Mater. Sci.* **2021**, *56*, 108–135. [CrossRef]
16. Voisiat, B.; Aguilar-Morales, A.I.; Kunze, T.; Lasagni, A.F. Development of an analytical model for optimization of direct laser interference patterning. *Materials* **2020**, *13*, 200. [CrossRef] [PubMed]

17. Milles, S.; Voisiat, B.; Nitschke, M.; Lasagni, A.F. Influence of roughness achieved by periodic structures on the wettability of aluminum using direct laser writing and direct laser interference patterning technology. *J. Mater. Process. Technol.* **2019**, *270*, 142–151. [CrossRef]
18. Grützmacher, P.G.; Profito, F.J.; Rosenkranz, A. Multi-Scale Surface Texturing in Tribology—Current Knowledge and Future Perspectives. *Lubricants* **2019**, *7*, 95. [CrossRef]
19. Soldera, M.; Alamri, S.; Storm, S.; Kunze, T.; Lasagni, A.F. Maximizing the efficiency of laser-fabricated diffraction gratings on PET using direct laser interference patterning. In Proceedings of the Laser-Based Micro- and Nanoprocessing XIV, San Francisco, CA, USA, 1–6 February 2020; p. 34. [CrossRef]
20. Baburaj, E.G.; Starikov, D.; Evans, J.; Shafeev, G.A.; Bensaoula, A. Enhancement of adhesive joint strength by laser surface modification. *Int. J. Adhes. Adhes.* **2007**, *27*, 268–276. [CrossRef]
21. Costil, S.; Convert, L.; Bourillot, E.; Pocholle, N.; François, M. Laser Texturing as Interfacial Treatment for Enhancing the Material Behaviors—The Real Influence of the Laser Treatment. In Proceedings of the Thermal Spray Proceedings, ITSC2023, Québec, QC, Canada, 22–25 May 2023; Paper No. ITSC2023P0428. pp. 428–435. [CrossRef]
22. Zhang, X.; Wang, R.; Meng, S.; Chen, W.; Zhou, L.; He, W.; Pan, X. Advances and Perspectives in Laser Texturing for Adhesion Enhancement: A Comprehensive Research Progress. *Prog. Surf. Sci.* **2025**, *100*, 100781. [CrossRef]
23. Wojdat, T.K.; Piwowarczyk, T. Influence of Laser Micro-Texturing and Plasma Treatment on Adhesive Bonding Properties of WC-Co Carbides with Steel. *Materials* **2024**, *17*, 5999. [CrossRef]
24. Wu, H.; Ye, J.; Chen, C.; Zhang, L.; Zhao, J.; Zhu, Z.; Jiang, Z. Effect of Laser Surface Texturing on Adhesive Properties of Electronic Labels. *Appl. Laser* **2023**, *43*, 112–119. [CrossRef]
25. Khan, M.A.; Halil, A.M.; Abidin, M.S.Z.; Hassan, M.H.; Ab Rahman, A.A. Influence of laser surface texturing on adhesive bonding: A comprehensive review on surface morphology and strength enhancement. *Opt. Laser Technol.* **2025**, *191*, 113339. [CrossRef]
26. Tofil, S.; Kurp, P.; Manikandan, M. Surface Laser Micropatterning of Polyethylene (PE) to Increase the Shearing Strength of Adhesive Joints. *Lubricants* **2023**, *11*, 368. [CrossRef]
27. Tofil, S.; Manoharan, M.; Natarajan, A. Surface Laser Micropatterning of Polyethylene Terephthalate (PET) to Increase the Shearing Strength of Adhesive Joints. *Mater. Res. Proc.* **2022**, *24*, 27–33. [CrossRef]
28. Tofil, S.; Antoszewski, B.; Mulczyk, K. The Efficiency of UV Picosecond Laser Processing in the Shaping of Surface Structures on Elastomers. *Polymers* **2020**, *12*, 2041. [CrossRef] [PubMed]
29. Witkowski, G.; Tofil, S.; Mulczyk, K. Effect of laser beam trajectory on pocket geometry in laser micromachining. *Open Eng.* **2020**, *10*, 830–838. [CrossRef]
30. Kromer, R.; Raoelison, R.N.; Danlos, Y.; Verdy, C.; Costil, S.; Liao, H. Adhesion Strength Improvement by Laser Surface Texturing of Metallic Repair Coatings Deposited by Cold Spraying. In Proceedings of the Thermal Spray Proceedings, ITSC2021, Virtual, 24–28 May 2021; Paper No. ITSC2021P0241. pp. 241–246. [CrossRef]
31. Hussein, F.I.; Akman, E.; Oztoprak, B.G.; Gunes, M.; Gundogdu, O.; Kacar, E.; Hajim, K.I.; Demir, A. Evaluation of PMMA joining to stainless steel 304 using pulsed Nd:YAG laser. *Opt. Laser Technol.* **2013**, *49*, 143–152. [CrossRef]
32. Roesner, A.; Scheik, S.; Olowinsky, A.; Gillner, A.; Reisgen, U.; Schleser, M. Laser assisted joining of plastic metal hybrids. *Phys. Procedia* **2011**, *12*, 370–377. [CrossRef]
33. Roesner, A.; Olowinsky, A.; Gillner, A. Long term stability of laser joined plastic metal parts. *Phys. Procedia* **2013**, *41*, 169–171. [CrossRef]
34. Yuce, C.; Karpat, F.; Yavuz, N.; Dogan, O. A review on advanced joining techniques of multi material part manufacturing for automotive industry. In Proceedings of the Eighteenth TheIIER International Conference, Rome, Italy, 28–29 March 2015.
35. Hopmann, C.; Kreimeier, S.; Keseberg, J.; Wenzlau, C. Joining of metal-plastics-hybrid structures using laser radiation by considering the surface structure of the metal. *J. Polym.* **2016**, *2016*, 4734913. [CrossRef]
36. Bergmann, J.P.; Stambke, M. Potential of Laser-manufactured Polymermetal hybrid Joints. *Phys. Procedia* **2012**, *39*, 84–91. [CrossRef]
37. Schricker, K.; Stambke, M.; Bergmann, J.P.; Brautigam, K.; Henckell, P. Macroscopic surface structures for polymer-metal hybrid joints manufactured by laser based thermal joining. *Phys. Procedia* **2014**, *56*, 782–790. [CrossRef]
38. Bauernhuber, A.; Markovits, T. Investigating thermal interactions in the case of laser assisted joining of PMMA plastic and steel. *Phys. Procedia* **2014**, *56*, 811–817. [CrossRef]
39. Katayama, S.; Kawahito, Y. Laser direct joining of metal and plastic. *Scr. Mater.* **2008**, *59*, 1247–1250. [CrossRef]
40. Lambiase, F.; Liu, F. Recent Advances in Metal–Polymer Joining Processes. In *Joining Processes for Dissimilar and Advanced Materials*; Elsevier: Amsterdam, The Netherlands, 2022; pp. 123–151. [CrossRef]
41. Lambiase, F.; Scipioni, S.I.; Lee, C.-J.; Ko, D.-C.; Liu, F. A State-of-the-Art Review on Advanced Joining Processes for Metal–Composite and Metal–Polymer Hybrid Structures. *Materials* **2021**, *14*, 1890. [CrossRef] [PubMed]

42. Paranjpe, N.; Uddin, M.N.; Rahman, A.S.; Asmatulu, R. Effects of Surface Treatment on Adhesive Performance of Composite-to-Composite and Composite-to-Metal Joints. *Processes* **2024**, *12*, 2623. [CrossRef]
43. Danielewski, H.; Skrzypczyk, A.; Tofil, S.; Witkowski, G.; Rutkowski, S. Numerical Simulation of Laser Welding Dissimilar Low Carbon and Austenitic Steel Joint. *Open Eng.* **2020**, *10*, 491–498. [CrossRef]
44. METINVEST S355JR Steel Data Sheet. Available online: https://metinvestholding.com/pl/products/steel-grades/s355jr/ (accessed on 9 March 2026).
45. *PN-EN 10025-2:2019-11*; Wyroby Walcowane na Gorąco ze Stali Konstrukcyjnych—Część 2: Warunki Techniczne Dostawy Stali Konstrukcyjnych Niestopowych (In English—Hot-Rolled Products from Structural Steels—Part 2: Technical Delivery Conditions for Non-Alloy Structural Steels). PKN (Polski Komitet Normalizacyjny): Warsaw, Poland, 2019.
46. Plastem. Polyamide PA66 Data Sheet. Available online: https://www.plastem.pl/oferta/tworzywa-sztuczne/poliamid-pa/ (accessed on 11 February 2026).
47. MULTIBOND-1101 Data Sheet. Available online: www.multibond.pl (accessed on 11 February 2026).
48. Elleb, R.; Engel, T.; Antoni, F.; Fontaine, J.; Mermet, F.; Poncin-Epaillard, F. Study of femtosecond laser multi-scale textured steel surfaces on the wettability in relation to aging. *J. Mater. Sci.* **2021**, *56*, 20169–20180. [CrossRef]
49. *PN-EN ISO 6892-1:2020-05*; Próba Rozciągania—Część 1: Metoda Badania w Temperaturze Pokojowej (In English—Tensile Test—Part 1: Test Method at Room Temperature). PKN (Polski Komitet Normalizacyjny): Warsaw, Poland, 2022.
50. *PN-EN ISO 291:2010*; Tworzywa Sztuczne—Znormalizowane Warunki Klimatyczne Kondycjonowania i Badania (In English–Plastics–Standardized Climatic Conditioning and Testing). PKN (Polski Komitet Normalizacyjny): Warsaw, Poland, 2010.
51. Mauclair, C.; Najih, B.; Comte, V.; Bourquard, F.; Delaigue, M. Dynamic spatial beam shaping for ultrafast laser processing: A review. *Opto-Electron. Sci.* **2025**, *4*, 250002. [CrossRef]
52. Stribick, S.; Alhadad, B. Laser Surface Texturing for Surface Preparation of Adhesive Bonding of Polypropylene. *Int. J. Adv. Manuf. Technol.* **2025**, *140*, 4339–4354. [CrossRef]
53. Siciliani, V.; Pelaccia, R.; Castagnetti, D.; Raimondi, L.; Donati, L.; Orazi, L.; Alfano, M. Enhancing the Shear Strength of Adhesive-Bonded Compression-Molded CFRP Laminates Using Selective UV Picosecond Laser Treatment. *Int. J. Adv. Manuf. Technol.* **2025**, *141*, 5697–5708. [CrossRef]
54. Hirakawa, R.; Terasaki, N.; Horiuchi, S.; Hartwig, S.; Gundlach, C.; Steinberg, J. Effect of Laser Surface Treatment Conditions on the Static and Fatigue Bonding Strength of Galvanised Steel Sheet. *J. Adhes.* **2026**, *102*, 1–23. [CrossRef]
55. Chey, S.Y.; Hong, S.; Kim, D.H.; Ahn, S.-H. The Effect of Laser Structuring on Hot-Press Joined Metal-Polymer Cross Tension Joints. *Int. J. Precis. Eng. Manuf.* **2025**, *26*, 961–976. [CrossRef]